



저작자표시-비영리-변경금지 2.0 대한민국

이용자는 아래의 조건을 따르는 경우에 한하여 자유롭게

- 이 저작물을 복제, 배포, 전송, 전시, 공연 및 방송할 수 있습니다.

다음과 같은 조건을 따라야 합니다:



저작자표시. 귀하는 원저작자를 표시하여야 합니다.



비영리. 귀하는 이 저작물을 영리 목적으로 이용할 수 없습니다.



변경금지. 귀하는 이 저작물을 개작, 변형 또는 가공할 수 없습니다.

- 귀하는, 이 저작물의 재이용이나 배포의 경우, 이 저작물에 적용된 이용허락조건을 명확하게 나타내어야 합니다.
- 저작권자로부터 별도의 허가를 받으면 이러한 조건들은 적용되지 않습니다.

저작권법에 따른 이용자의 권리는 위의 내용에 의하여 영향을 받지 않습니다.

이것은 [이용허락규약\(Legal Code\)](#)을 이해하기 쉽게 요약한 것입니다.

[Disclaimer](#)

Patient-derived organoid model for
prediction of cancer-risk in patient with
germline mutation of mismatch repair
genes

Youmi Shin

Department of Medical Science

The Graduate School, Yonsei University

Patient-derived organoid model for
prediction of cancer-risk in patient with
germline mutation of mismatch repair
genes

Directed by Professor Tae Il Kim

The Master's Thesis
submitted to the Department of Medical Science,
the Graduate School of Yonsei University
in partial fulfillment of the requirements for the degree of
Master of Medical Science

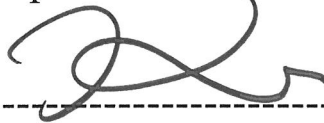
Youmi Shin

June 2022

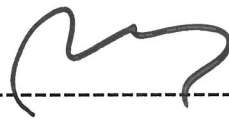
This certifies that the Master's Thesis of
Youmi Shin is approved.



Thesis Supervisor : Tae Il KIM



Thesis Committee Member#1 : Hyunki Kim



Thesis Committee Member#2 : Ki Taek Nam

The Graduate School
Yonsei University

June 2022

ACKNOWLEDGEMENTS

졸업을 앞두고, 어느새 이렇게 시간이 빨리 지나갔음을 느낍니다. 모든 학위과정 학생들이 그렇듯 많은 걱정과 좌절 그리고 실패를 경험했지만 저를 도와주셨던 많은 분들 덕분에 이겨낼 수 있었던 것 같습니다. 학위과정이 짧다면 짧고, 길다면 길지만 이 시간이 단순한 학위뿐만이 아닌 앞으로 제 삶에 큰 밑거름이 될 것 같다는 사실이 제게 큰 가치가 된 것 같습니다.

먼저, 부족한 저를 많은 이해와 보살핌으로 지금까지 이끌어주시고 지도해주신 김태일 교수님께 감사드립니다. 저에게 배움의 기회를 주심에 감사드리고 앞으로 교수님께서 주신 기회와 가르침을 잊지않고 연구에 임하면서 발전하는 연구자가 되도록 노력하겠습니다.

제 연구에 도움을 주시고 친절히 아낌없는 조언과 힘이 되는 말씀해주신 김현기 교수님, 마찬가지로 심사를 맡아주시고 세심한 조언해주신 남기택 교수님께 감사드립니다.

제 학위과정을 처음부터 가장 가까이에서 저와 함께 해주신 유정언니에게 감사드립니다. 실험을 지도해주시고 조언을 아끼지 않아주셔서 이에 많은 자극도 받고, 배움을 얻을 수 있었습니다. 저에게 있어 존경스러운 선배임과 동시에 제 인생의 좋은 언니가 되어주셔서 감사드립니다. 마찬가지로, 저에게 많은 조언과 도움 주신 김동건 박사님께 감사드립니다. 언제나 실험에 대해 함께 고민해주시고 논의해주셔서 박사님의 도움으로 끝까지 마무리할 수 있었습니다. 학위과정 동안 두 분의 애정 어린 보살핌 덕분에 힘든 시간들 속에서도 포기하거나 무너지지 않고 이겨 낼 수 있었습니다.

저에게 없어서는 안되는 친구들, 지금까지 제 인생에 많은 부분을 차지했고 앞으로도 마찬가지로 은주와 주심이에게 감사의 인사를 전합니다. 항상 서로의 일상을 공유하며, 슬픔과 기쁨 그 모든 순간을 함께 해주어서 고맙고 저에게 많은 의지가 되어준 것처럼 저도 언제나 그들의 곁에 있겠다고 전해주고 싶습니다. 항상 먼저 연락해주고 응원을 아끼지

않아주었던 민정에게도 지금까지 말로 전한적은 없지만 고맙다고 전하고 싶습니다. 그리고 같은 학위과정 학생으로서 많이 의지하고 도움 받은 수빈언니에게 많은 응원과 감사의 인사를 전합니다.

마지막으로, 저의 진학을 믿음과 사랑으로 지지해준 가족들에게 감사드립니다. 가족들의 보살핌과 지원 없이는 불가능했고, 항상 저를 많은 사랑으로 보듬어 주심에 감사드리고 그 사랑을 베풀 수 있는 사람이 되겠습니다.

<TABLE OF CONTENTS>

ABSTRACT	1
I. INTRODUCTION	3
II. MATERIALS AND METHODS	6
1. Human organoid culture and measurement of organoid growth ·	6
2. Drug treatment	6
3. Immunofluorescence and DNA damage quantification in organoids	7
4. Immunohistochemistry	7
5. Western blot	8
6. Evaluation of MNNG-induced mutations in organoids	8
7. Whole Genome Sequencing	9
III. RESULTS	10
1. Mismatch Repair (MMR) pathway	10
2. Generation of the DNA damage lesion using methylating agent, MNNG	12
3. The effect of MNNG on growth of human normal colon organoids	14
4. Repair of the DNA damage lesion by O-6-methylguanine-DNA methyltransferase (MGMT) and induction of apoptosis by ATR inactivation	18
5. The growth inhibition of MNNG-treated normal organoids by additional treatment of ATR inhibitor and O ⁶ BG	20
6. No change of organoid growth by combined treatment of MNNG, ATR inhibitor and O ⁶ BG in Lynch syndrome patient-derived organoids	24
7. γ H2AX expression as a key marker of DNA damage response	28

8. DNA Damage Responses (DDR) of PDOs to MNNG and O ⁶ BG	30
9. MNNG-induced mutation accumulation in normal organoids and LS-PDOs	47
10. Whole genome sequence analysis in MNNG-treated organoids and MLH1 mutated PDOs	41
IV. DISCUSSION	44
V. CONCLUSION	47
REFERENCES	48
ABSTRACT (IN KOREAN)	50

LIST OF FIGURES

Figure 1. O ⁶ meG-T mismatch repair pathway	11
Figure 2. Repair of O ⁶ meG lesions created upon exposure to S _N 1 DNA alkylating agents	13
Figure 3. The effect of MNNG on growth of human normal colon organoids	15
Figure 4. Increased MNNG-induced cell death by additional inhibition of MGMT and ATR	19
Figure 5. Growth suppression of normal organoids by combined treatment of MNNG, ATR inhibitor and O ⁶ BG	21
Figure 6. No effect of combined treatment of MNNG, ATR inhibitor and O ⁶ BG on growth of MMR gene mutated PDOs	25
Figure 7. γ H2AX, key molecular marker of DNA damage response	29
Figure 8. γ H2AX expression after treatment of MNNG and O ⁶ BG in normal and LS-PDOs	31
Figure 9. MNNG-induced single Nucleotide Variants(SNVs) in normal organoids and LS-PDOs	38
Figure 10. MNNG-induced mutation accumulation in normal and MLH1 mutated PDOs	42

LIST OF TABLES

Table 1. Primer sequences for CpG island in APC gene	40
--	----

ABSTRACT

Patient-derived organoid model for prediction of cancer-risk in patient with germline mutation of mismatch repair genes

Youmi Shin

*Department of Medical Science
The Graduate School, Yonsei University*

(Directed by Professor Tae Il Kim)

About 10~15% of Colorectal cancer (CRC) shows MSI-tumor, and about 20% of MSI-tumor is caused by germline mutation of Mismatch repair (MMR) genes MLH1, MSH2, MSH6, PMS2, and EPCAM, which is known as Lynch syndrome (LS) or Hereditary Non-polyposis Colorectal Cancer Syndrome (HNPCC).

Although Lynch syndrome patients have a high risk of colorectal cancer, not all of them have the same risk of developing CRC even in the same pathogenic germline mutations of MMR gene. We suggest the individualized prediction model for CRC risk using Lynch syndrome patient-derived organoid (PDO).

First of all, we measured organoid response to the cytotoxic effect of a methylating agent, N-Methyl-N'-Nitro-N-Nitrosoguanidine (MNNG), based on the DNA damage induced apoptosis. We treated colon organoids with various dose and period of MNNG. However, we could not find significantly rapid change of normal organoid growth. Then, to increase the effect of MNNG with induction of apoptosis in colon organoids, we additionally treated O⁶BG, MGMT inhibitor, and ATR inhibitor. We found that the cytotoxic effect by combined treatment of MNNG, O⁶BG and ATR inhibitor in normal organoids were higher than MMR gene mutated organoids, which was detected after several passage of organoids. Next, for early detection of differential change between normal organoids and LS-PDOs, we examined DNA damage response by analyzing the expression of γ H2AX, which is a DNA damage recognition marker for detecting in earlier phase of DNA damage. Then, after treatment of MNNG and O⁶BG we found a higher expression of γ H2AX in normal

organoids than in the MMR gene mutated organoids.

To identify the mutations that accumulated by MNNG, we performed the analysis of the Sanger Sequence and Whole Genome Sequence (WGS). We treated MNNG in colon organoids and harvest with several recovery times. We found that normal organoids showed decreased base transitions over time, however, LS-PDOs showed increased base transitions over time. In addition, according to analysis of WGS data, MNNG-induced mutation number was significantly increased in MLH1 gene mutated organoids, compared to normal organoids.

In conclusion, the measurement of DNA damage response by MNNG and O⁶BG in Lynch syndrome patient-derived organoid model could serve as an individualized prediction model of CRC risk in Lynch syndrome patients.

Key words: Patient-derived organoids, Colorectal cancer, Lynch Syndrome, DNA damage response, MNNG

Patient-derived organoid model for prediction of cancer-risk in patient with germline mutation of mismatch repair genes

Youmi Shin

*Department of Medical Science
The Graduate School, Yonsei University*

(Directed by Professor Tae Il Kim)

I. INTRODUCTION

Colorectal cancer (CRC) is the third most common cause of cancer-related deaths worldwide.¹ Approximately 65% of CRC cases are sporadic with no family history or apparent genetic predisposition. The majority of sporadic CRCs (~85%) show chromosomal instability (CIN), with changes in chromosome number or structure. These changes involve the gain or loss of chromosome segments and the loss of heterozygosity (LOH), which then cause gene copy number variations (CNVs). These alterations activate the expression of tumor-related genes and the pathways essential for CRC initiation and progression.² The remaining cases (~15%) have high-frequency microsatellite of instability (MSI) phenotypes. Microsatellite Instability-High (MSI-H) status shows certain sections of microsatellites that have become unstable, since the major mismatch repair (MMR) genes are not functioning properly. The majority of sporadic MSI-H CRC is caused by the hypermethylated promoter of the MLH1 gene and about 20% of MSI-H tumor is from the germline mutation of the MMR genes (MLH1, MSH2, MSH6, PMS2 and EPCAM), which is known as Lynch syndrome (LS) or Hereditary Non-Polyposis Colorectal Cancer Syndrome (HNPCC).³

Identifying patients with Lynch syndrome is clinically important because it is the most common cause of hereditary CRC. Individuals with Lynch syndrome tend to

have fewer than ten adenomatous polyps cumulatively in their life. Adenomas are commonly seen in patients younger than the age of 40 and frequently have a villous growth pattern with moderate to high-grade dysplasia. Adenomas in individuals with Lynch syndrome tend to transform into cancers more rapidly than those in individuals of the general population.⁴

Lynch Syndrome patients have a 60–80% lifetime risk of developing CRC and other tumors, including endometrial and ovarian cancer, urologic cancer, and gastric cancer that typically develop around the fifth decade of life and are characterized by MSI-H and the loss of expression of the corresponding MMR protein MLH1, MSH2, MSH6, PMS2, or EPCAM.³ Mutations in the MLH1 or MSH2 gene tend to lead to a higher risk (70 to 80%) of developing cancer in a person's lifetime, while mutations in the MSH6 or PMS2 gene have a relatively lower risk (25 to 60%) of cancer development.⁵

Consequently, most Lynch syndrome patients genetically carry a mutation in one allele of their MMR genes. However, 30% of lynch syndrome patients have a variant of uncertain (or unknown) significance (VUS). It is a genetic variant that has been identified through genetic testing, whose significance to an organism's function or health is not yet unknown. That means whose impact on the individual's cancer risk is not yet known.⁶ Therefore, VUS represents a major clinical challenge because Lynch Syndrome diagnosis of carriers and their relatives is impossible due to lack of satisfying significance.

In addition, although Lynch syndrome patients have a high risk of colorectal cancer, not all of them have the same risk of developing CRC. However, there is no way to evaluate the difference in cancer or tumor risk among Lynch syndrome patients. Even in the same pathogenic germline mutations of the MMR gene, individualized risk of cancer development is various, suggesting the necessity of an individualized prediction model for cancer risk.

As for the functional assay of MMR genes and their variants, some models using

classical cell line and animal model in biomedical research has been successful in the research field of molecular mechanism and biologic significance.⁷ However, these results could not explain the individual difference in cancer risk in Lynch syndrome. Recently, with the advent of human organoids, it has become possible to recreate the architecture and physiology of human organs in remarkable detail. Human organoids have been used to study infectious diseases, genetic disorders, and cancers through the genetic engineering of human cells. Therefore, the human organoids can provide valuable information about the mechanisms of specific diseases and a patients-specific in vitro disease model, in addition to their potential application in pharmaceutical drug testing and molecular medicine.

Therefore, we developed the patient-derived organoid model to measure the biological significance of MMR gene variants and predict cancer risks in individual Lynch syndrome patients.

II. MATERIALS AND METHODS

1. Human organoid culture and measurement of organoid growth.

Human colon organoids were derived from normal tissues of a resected colon segment of patients diagnosed with colorectal cancer and from endoscopy material of healthy Lynch syndrome patients. The tissues from patients were washed three times with PBS and cut into pieces. Subsequently, the fragments were incubated in a digestion solution (DMEM with collagenase). After incubation for 30~40 minutes at 37°C, they were pipetted to liberate the crypts. Then add PBS and centrifuge at 1,500 rpm for 3 minutes. Isolated crypts were pelleted and cultured in domes with Matrigel (Corning) then add organoid culture medium. The composition of organoid culture medium is: Basal culture medium with 50% Wnt/R-Spondin conditioned medium, 10% Noggin, B27 and N2 supplements (Gibco), n-Acetyl Cysteine (Sigma-Aldrich), Nicotinamide (Sigma-Aldrich), human EGF, Gastrin (Sigma-Aldrich), A83-01 (Sigma-Aldrich), SB202190 (Sigma-Aldrich), and Primocin (InvivoGen). Organoid culture medium was refreshed every two days. To passage the organoids, Matrigel was broken up by pipetting and organoids were collected in a tube. The organoids were centrifuged at 1,500 rpm for 3 min and the medium removed. 400 μ l Triple Express (Invitrogen) was added and the organoids were incubated at 37°C for approximately 5 min. Medium was added with 10 μ M Y27632 (Sigma-Aldrich) for the first 2 days. The ten organoids were counted which the size was over 50 μ m in initial day for measurement of growth.

2. Drug treatment

The organoids were exposed to N-Methyl-N'-Nitro-N-Nitrosoguanidine (MNNG) (Tokyo Chemical Industry co.). To exclude differences in the efficacy of MNNG due to O⁶-methylguanine-DNA methyltransferase (MGMT) activity, cells were exposed to 25 μ M O⁶-Benzylguanine (O⁶BG) (Sigma-Aldrich) and 10 μ M ATR inhibitor (Sigma-Aldrich) was also used to induce apoptosis. After the organoids were pre-treated with O⁶-benzylguanine, they were treated with 15 μ M and 25 μ M MNNG for

45 minutes, 24 hours and 48 hours, and ATR inhibitor treated for 20 hours. All chemicals were dissolved in dimethyl sulfoxide and diluted in deionized water.

3. Immunofluorescence and DNA damage measurement in organoids

The organoid culture media was removed, and the organoid was fixed with 4% paraformaldehyde (PFA) for 30 minutes at room temperature. Then they were washed extensively at least 3 times with PBS for removal of the fixing solution. For staining, organoids were permeabilized with 5% Triton-X for 20 minutes at room temperature. The organoids were blocked with 3% BSA in PBS for 1 hour at room temperature. Then, they were incubated with rabbit anti- γ H2AX primary antibody (cell signaling, #9718) overnight at 4°C in 1:500 dilution. The organoids were washed several times with PBS and incubated with secondary anti-rabbit antibodies for 1 hour at room temperature in the dark and washed again with PBS. The organoids were washed, DAPI was added and washed again with PBS. The organoids were analyzed with an LSM700 laser scanning confocal microscope (Carl Zeiss) and Operetta CLS (PerkinElmer).

4. Immunohistochemistry

The organoids stained for γ H2AX was performed on 4 μ m sections of 4% PFA fixed, paraffin-embedded. The paraffin embedded sections were deparaffinized in xylene and rehydrated in gradually decreasing concentrations of ethanol. Antigen retrieval was performed using sodium citrated buffer (10mM, pH 6.0) in a heated pressure cooker for 5 or 7 minutes. After incubation with 3% hydrogen peroxide for 30 minutes to block endogenous peroxidase activity, sections were incubated in a blocking reagent for 30 minutes at room temperature. Sections were incubated with the primary antibody overnight at 4°C, followed by the secondary antibody for 30 minutes at room temperature. After the slides had been developed with a Vectastain ABC kit (Vector Laboratories, Burlingame, CA, USA), immunodetection was performed using DAB solution (Dako, Carpinteria, CA, USA). After counterstaining with hematoxylin, IHC staining was evaluated by light microscopy and

immunoactivity was assessed based on the proportion of immunostained organoids.

5. Western blot

Samples were lysed using lysis buffer (50 mM Tris-HCl pH 8.0, 150 mM NaCl, 1% NP-40) containing protease inhibitors. Protein content was quantified using standard BCA assay (BioRad) and equal amounts of protein were run on polyacrylamide gels (15%) and transferred to PVDF membranes. After blocking with 10% skim milk in 0.1% TBST (Tween20 in TBS solution) for 60 minutes, membranes were probed with primary antibodies and incubated at 4°C overnight. Bound antibodies were detected with secondary antibody and visualized using West-Q Femto clean ECL solutions. For a loading control, the monoclonal anti- β -actin antibody (Genetex, GTX109639) at a dilution of 1:2,000 was used.

6. Evaluation of MNNG-induced mutations in organoids

After Organoids were exposed to MNNG, collected in cell recovery solution (Corning) and incubated at room temperature for 30 minutes with regular shaking in order to remove the Matrigel. The DNA from organoids was isolated using the DNeasy Blood & tissue kit (Qiagen) according to manufacturer's instructions. PCR was performed using AccuPower PCR Master Mix (Bioneer) according to manufacturer's protocol. Primer sequences: APC_CpG_1_for, 5'-AGACAAACAAGGATTTCCCGGAAGA-3', APC_CpG_1_rev, 5'-AGATGAACAATCATTTGCCAACAGA-3'; APC_CpG_2_for, 5'-TCATCACTCTGACAACCTCAGTGACT-3', APC_CpG_2_rev, 5'-GCTCCTCGCCATGAATATGCTC-3'. The PCR products were Sanger sequenced by Macrogen.

7. Whole Genome Sequencing (WGS) and Read Alignment

The samples were prepared according to the Illumina TruSeq Nano DNA library preparation guide or TruSeq DNA PCR-free library preparation guide. The libraries were sequenced using Illumina platform. DNA libraries for sequencing from 1 μ g of genomic DNA isolated from organoid by using the DNeasy Blood & tissue kit (Qiagen) according to manufacturer's instructions. First, paired-end sequences generated by the HiSeq instrument are mapped to the human genome using Isaac aligner (iSAAC-04.18.11.09) where the reference sequence is the UCSC assembly hg19 (original GRCh37 from NCBI, Feb. 2009).

III. RESULTS

1. Mismatch Repair (MMR) pathway

The MMR pathway primarily involves three steps: recognition, excision and resynthesis. In human cells, mismatch recognition is mediated predominantly by the heterodimer of hMSH2 and hMSH6, referred to as hMutS α .⁸ Initially, the MutS protein complex recognizes base–base mismatches and insertion–deletion loops. This mismatch-bound hMSH2/hMSH6 heterodimer undergoes an ATP-dependent conformational change, which converts it to a sliding clamp capable of translocating along the DNA backbone. The hMSH2/hMSH6 ATP DNA complex is bound by a second heterodimer MutL, composed of hMLH1 and hPMS2.⁹ This complex can translocate in either direction, in search of a strand discontinuity. The downstream consequences of these events include the induction of DNA damage signaling events, G2/M cell cycle arrest, induction of sister chromatid exchanges and apoptosis.¹⁰ If the DNA lesion is not repaired, DNA replication by either conventional or translesion DNA synthesis (TLS) polymerases can lead to the formation of O⁶meG-T mismatch. Recognition, following replication, of O⁶-meG:C or O⁶-meG:T mismatches by hMutSa and recruitment of hMutLa initiates futile cycles of excision repair. Replication past a gap left by removal of a mismatched T produces double strand breaks leading to cell death.

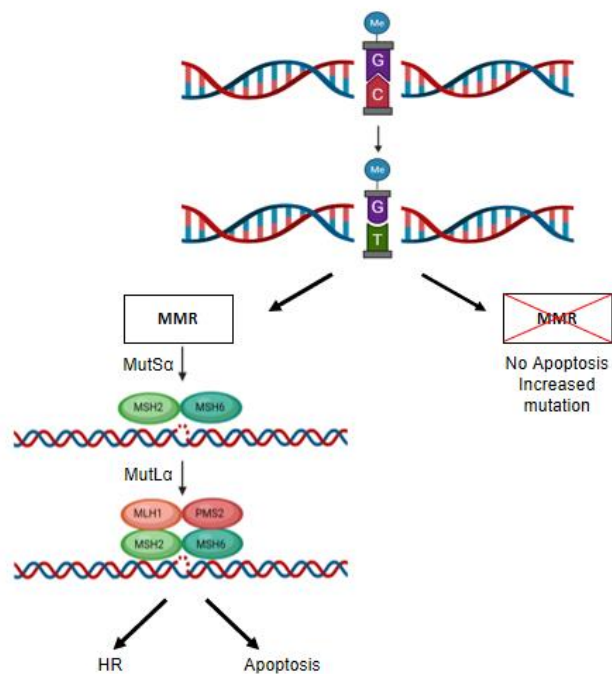


Figure 1. $O^6\text{meG-T}$ mismatch repair pathway. In MMR-deficient pathway, DNA mismatch escapes checkpoint signaling and accumulates G:C>A:T mutations at $O^6\text{-meG:T}$ sites during the following rounds of replication. The pathway results in cell survival but with mutation.¹¹

2. Generation of the DNA damage lesion using methylating agent, MNNG

The pattern of DNA lesions generated by an alkylating agent depends on the number of reactive sites within the alkylating agent, its particular chemical reactivity, the type of alkyl group addition and the DNA substrate.¹² The O⁶-position of guanine is a major site of methylation by S_N1 type alkylating agents for generating O⁶-methylguanine (O⁶-meG).¹³ The O⁶-meG pairs with thymine and induce the mismatch. Therefore, using SN1 type alkylating agent N-Methyl-N'-Nitro-N-Nitrosoguanidine (MNNG),¹⁴ induces the O⁶-meG lesion to generate DNA mispairs, then repairs the DNA lesion through the MMR pathway.¹¹

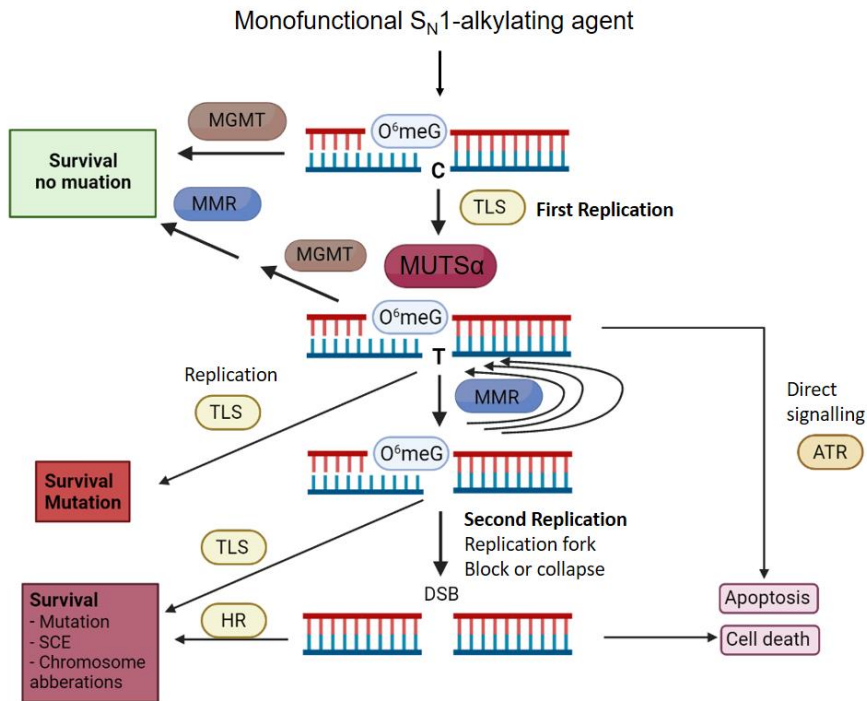
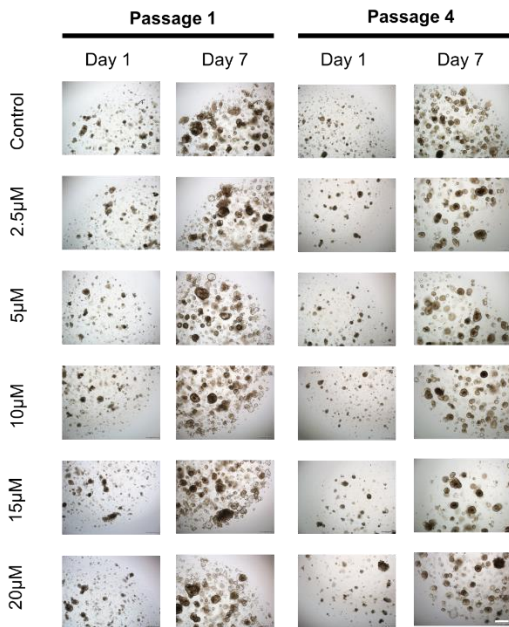


Figure 2. Repair of O^6 meG lesions created upon exposure to S_N1 DNA alkylating agents. S_N1 -alkylating agents generate the O^6 -methylguanine and formation of O^6 meG:T mispairs. $MUTS\alpha$ recognizes the mispairs and initiates the MMR pathway, leading to futile cycles of DNA resection. The process can cause replication fork collapse and double-strand break (DSB). The DSB can be repaired by homologous recombination (HR) pathway resulting in cell survival but with mutation, sister chromatid exchange (SCE) or chromosome aberrations.¹³ If the DSB is not repaired, it can induce cell death by apoptosis.

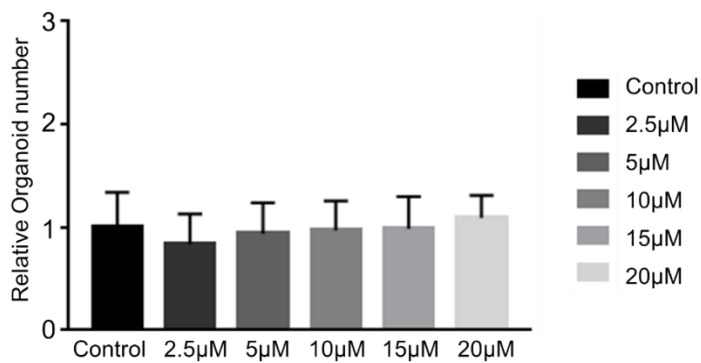
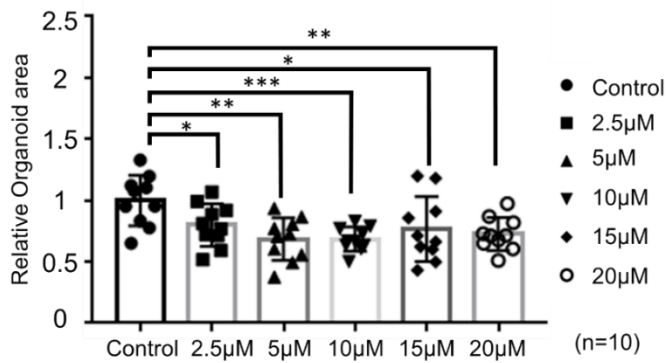
3. The effect of MNNG on growth of human normal colon organoids

The MMR process causes death of cells with methylation-damaged DNA bases. Therefore, to determine the proper dose and treatment time of MNNG for normal response as a control, we measured proportions of cell growth and death after treatment of the methylating agent, MNNG, in normal colon organoids. DNA lesion is caused by MNNG, which induces cell death through DNA damage. First of all, we treated high concentration (0, 2.5, 5, 15, 25 μM) of MNNG for short term (45 minutes) and low concentration (0, 0.5, 1, 1.5, 2.5 μM) for long term (48 hours).⁶ The normal organoids were derived from normal colon tissue of colorectal cancer patients with MSS molecular feature. We observed the organoid growth at every passage after the treatment of MNNG, and compared the area and number of organoids after four passage of organoids (figure3 A-D). The organoid growth relatively decreased in MNNG-treated normal organoids but there was no significant difference in organoid number. (figure3 A-D). In addition, there was no significant difference in organoid growth between high dose/short term treated and low dose/long term treated organoids.

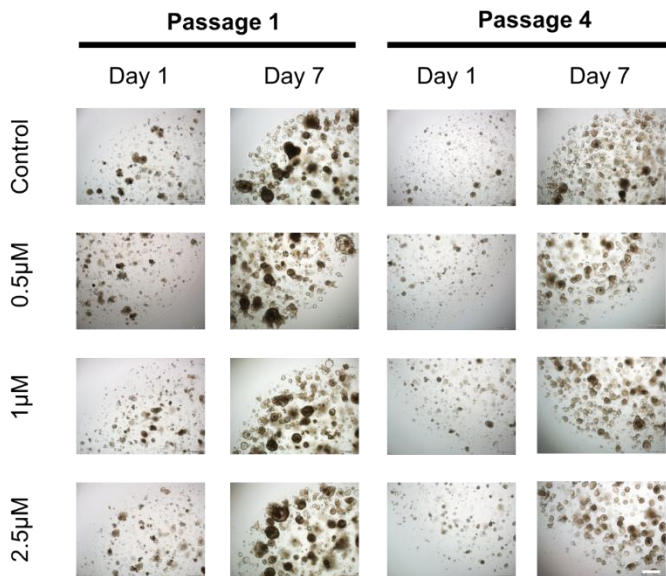
A.



B.



C.



D.

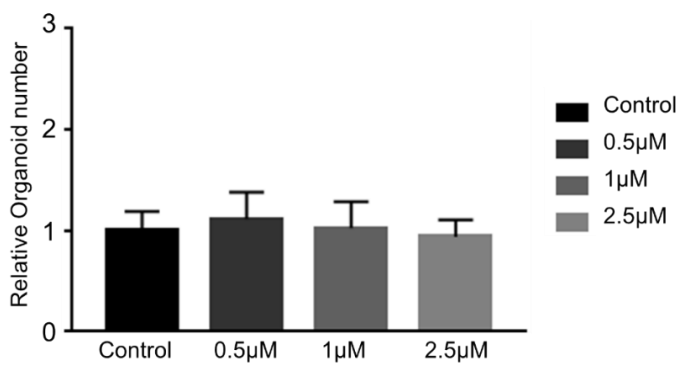
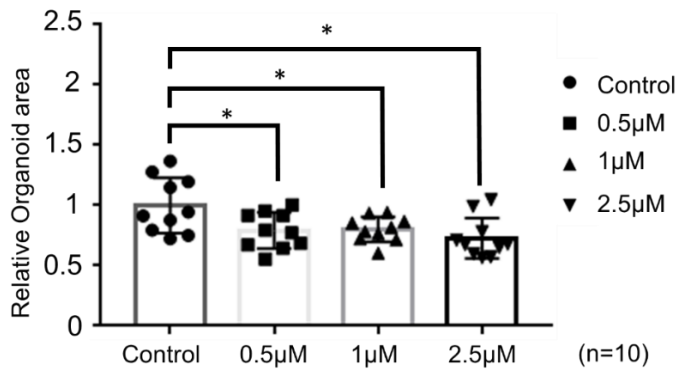


Figure 3. The effect of MNNG on growth of human normal colon organoids. (A, B) The MNNG was treated in concentration of 0, 2.5, 5, 15, 25 μ M for 45 minutes. (A) Representative bright-field images of organoids. Scale bar, 500 μ m. (B) The organoids area and number were measured after 4 passages of organoids. (C, D) The MNNG was treated in concentration of 0, 0.5, 1, 1.5, 2.5 μ M for 48 hours. (C) Representative bright-field images of organoids. Scale bar, 500 μ m. (D) The organoids area and number were measured after 4 passages of organoids. Data were expressed as the mean \pm standard error of three independent experiments; * $p < 0.05$, ** $p < 0.01$, and *** $p < 0.001$ (compared with the control).

4. Repair of the DNA damage lesion by O-6-methylguanine-DNA

methyltransferase (MGMT) and induction of apoptosis by ATR inactivation

The O⁶-meG lesion is repaired by MGMT, and if MGMT is sufficient for repairing the whole O⁶-meG lesions, the DNA mispairs are not made, and cells survive with no mutation.¹⁵ Therefore, additional usage of O⁶-Benzylguanine (O⁶BG), the inhibitor of MGMT, can increase the sensitivity of MNNG and lead it to become more dependent on the MMR pathway. After MMR system processes, the ATR-chk1 activation participates in damage repairing, then without ATR-Chk1 activation, the apoptosis is induced. Therefore, the treatment of ATR inhibitor can lead to cell death.¹⁶

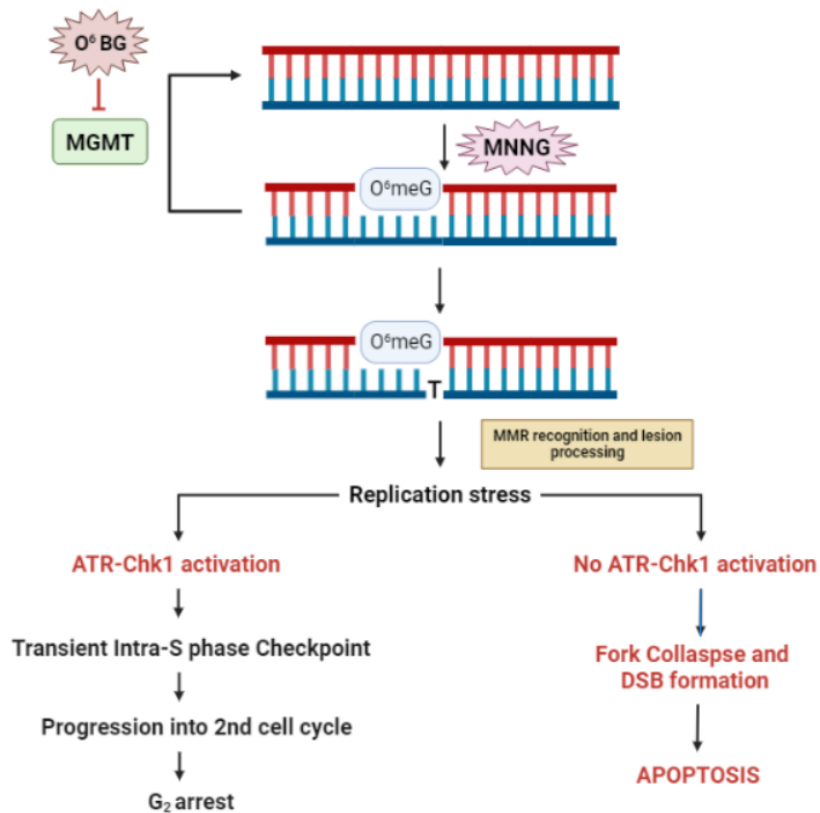
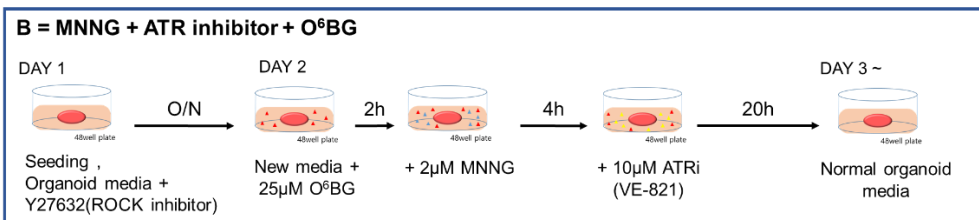
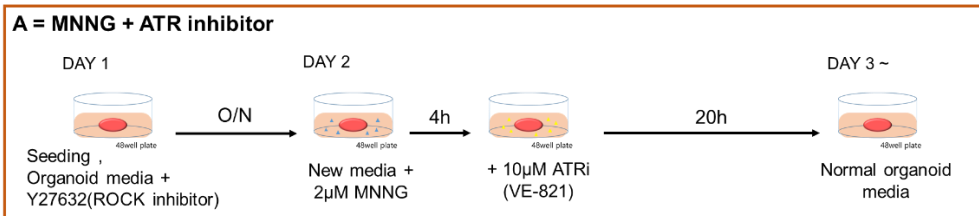


Figure 4. Increased MNNG-induced cell death by inhibition of MGMT and ATR. The O⁶-meG lesion can be directly repaired by O⁶-methylguanine-DNA methyltransferase (MGMT). Therefore, O⁶BG, the MGMT inhibitor, can increase MMR recognition and DNA lesion processing. Then, the MMR-dependent recognition of O⁶-meG:T can directly signal for cell death through the inhibition of ATR interacting pathway.

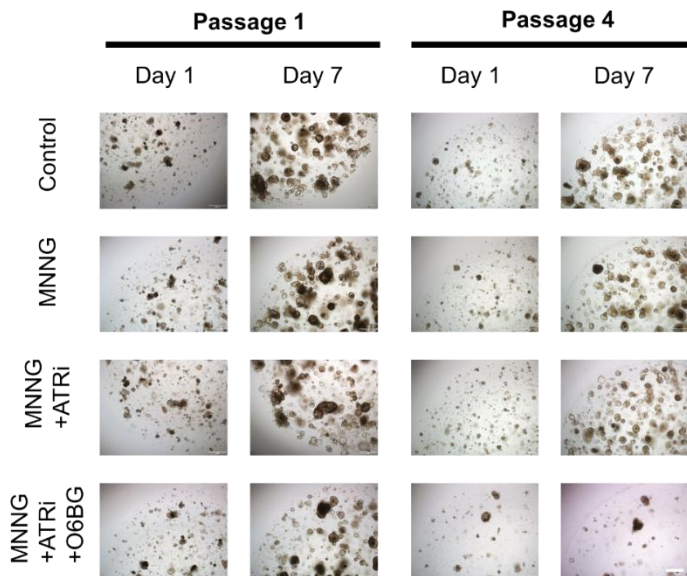
5. The growth inhibition of MNNG-treated normal organoids by additional treatment of ATR inhibitor and O⁶BG

To increase the sensitivity of MNNG and induce apoptosis in normal colon organoids, we additionally treated the O⁶BG and ATR inhibitor (figure 4). We found that both the growth and number of organoids significantly decreased after the combined treatment of MNNG, ATR inhibitor and O⁶BG in normal colon organoids (figure 5 B-C).

A.



B.



C.

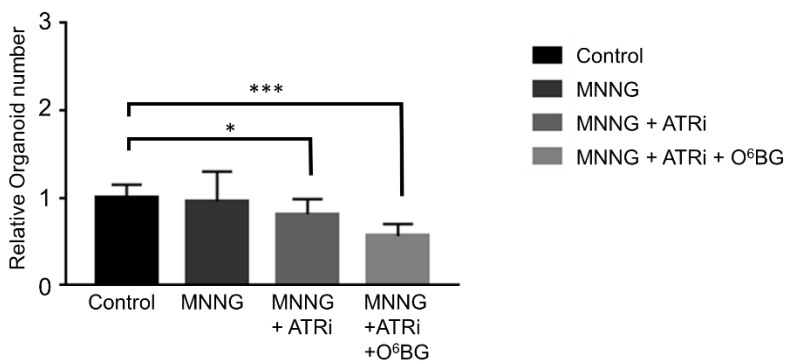
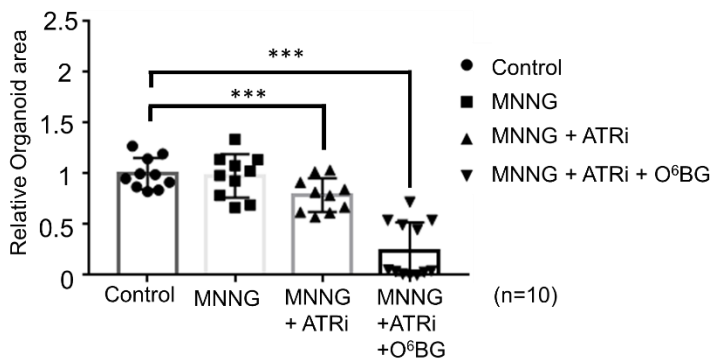
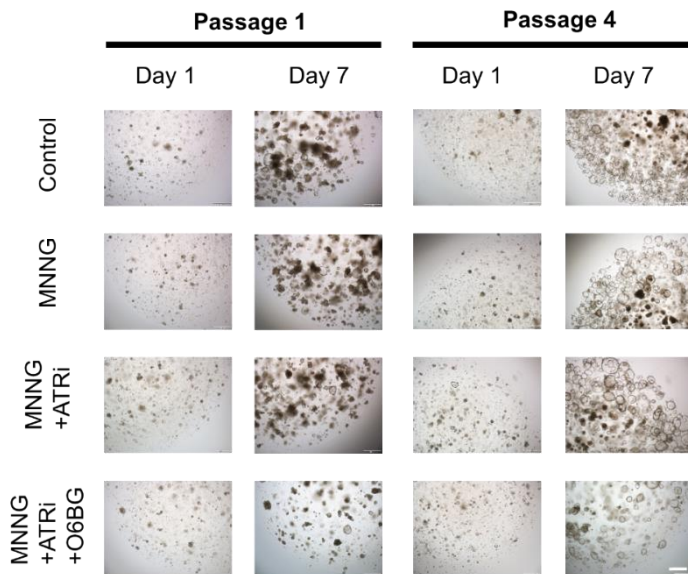


Figure 5. Growth suppression of normal colon organoids by combined treatment of MNNG, ATR inhibitor, and O⁶BG. (A) A schematic diagram of drug treatment. With the pretreatment of O⁶BG (25 μ M) for 2 hours, the MNNG was treated in concentration of 2 μ M for 24 hours, and 10 μ M of ATR inhibitor was treated. (B) Representative bright-field images of organoids after drug treatment. Scale bar, 500 μ m. (C) The organoids area and number were measured after 4 passages of organoids. Data were expressed as the mean \pm standard error of three independent experiments; * $p < 0.05$, ** $p < 0.01$, and *** $p < 0.001$ (compared with the control).

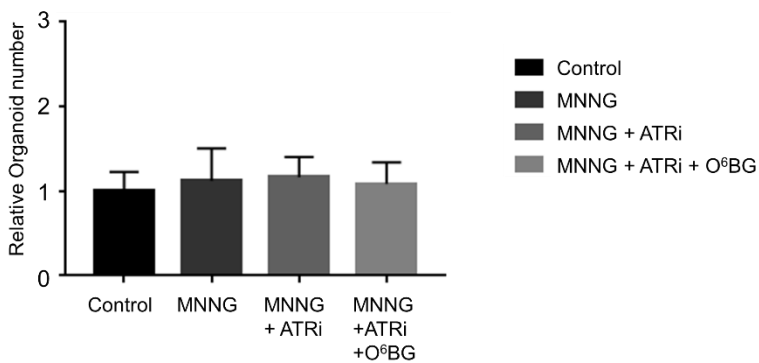
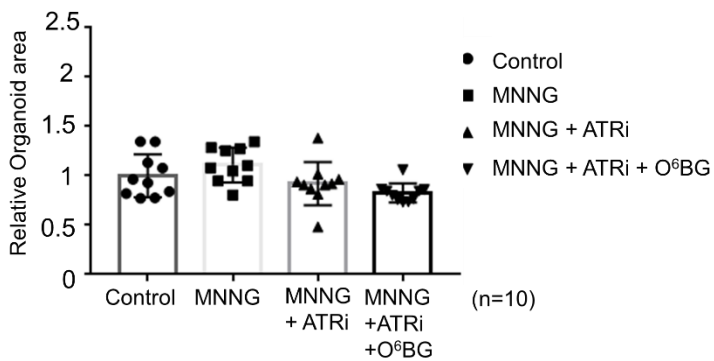
6. No change of organoid growth by the combined treatment of MNNG, ATR inhibitor and O⁶BG in Lynch syndrome patient-derived organoids

Next, we treated the MNNG, ATR inhibitor and O⁶BG in organoids derived from Lynch syndrome patients to confirm whether the MMR recognition of DNA lesion are working or not. (figure 6). Notably, there was no significant difference in organoid growth in both MLH1 and MSH2 mutated PDOs. These results suggest that the MMR-deficient organoids could escape the cytotoxic effect of combined agents because their MMR function was deficient.

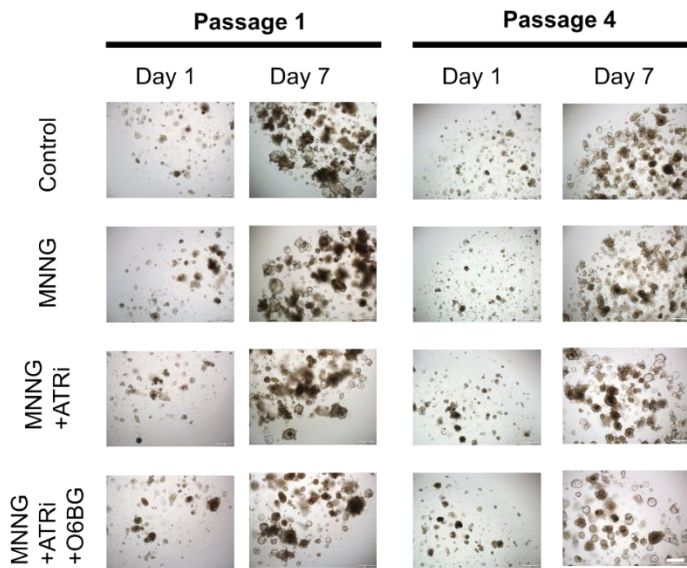
A.



B.



C.



D.

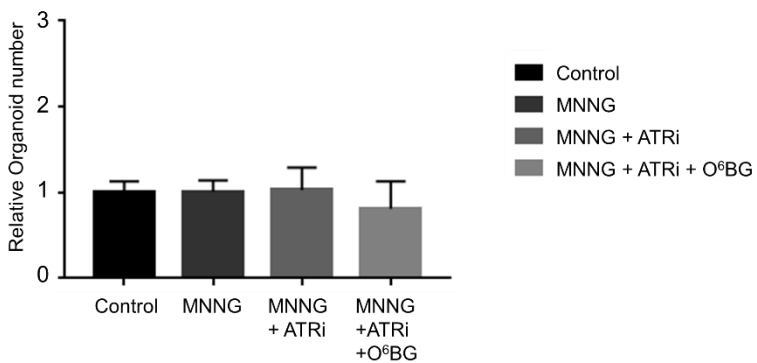
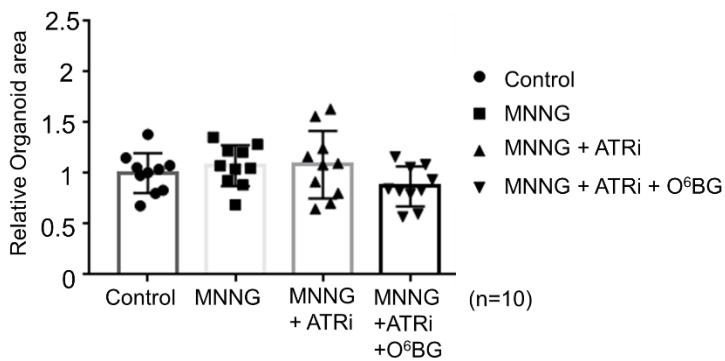


Figure 6. No effect of combined treatment of MNNG, ATR inhibitor and O⁶BG on growth of the MMR gene mutated PDOs. With the pretreatment of O⁶BG (25 μ M), the MNNG was treated in concentration of 2 μ M for 24 hours, then 10 μ M of ATR inhibitor was treated. MLH1 gene mutated LS-PDOs (A, B) and MSH2 gene mutated LS-PDOs (C, D) were treated with combined drugs. (A, C) Representative bright-field images after drug treatment. Scale bar, 500 μ m. (B, D) The organoids area and number were measured after 4 passages of organoids. Data were expressed as the mean \pm standard error of three independent experiments; * $p < 0.05$, ** $p < 0.01$, and *** $p < 0.001$ (compared with the control).

7. γ H2AX expression as a key marker of DNA damage response

Although we found a significant difference in the growth of PDOs through the combined treatment of MNNG, O⁶BG and ATR inhibitor, we could measure this difference after several passage of organoids. Therefore, we need to search a molecular marker, which can be detected in earlier phase of DNA damage. H2AX is a key marker in the repair process of damaged DNA.¹⁷ When DNA damage occurs, it is always followed by the phosphorylation of the histone H2AX, forming γ H2AX (figure 7). Detection of γ H2AX has emerged as a highly specific and sensitive molecular marker for monitoring DNA damage initiation and resolution. Quantitation of γ H2AX foci has been applied as a useful tool for the evaluation of DNA damages by various drugs. Therefore, measuring γ H2AX of MNNG-treated LS patient-derived organoids could be used for the evaluation of DNA damage by MMR deficiency, and its correlation with tumor risks in LS patients.

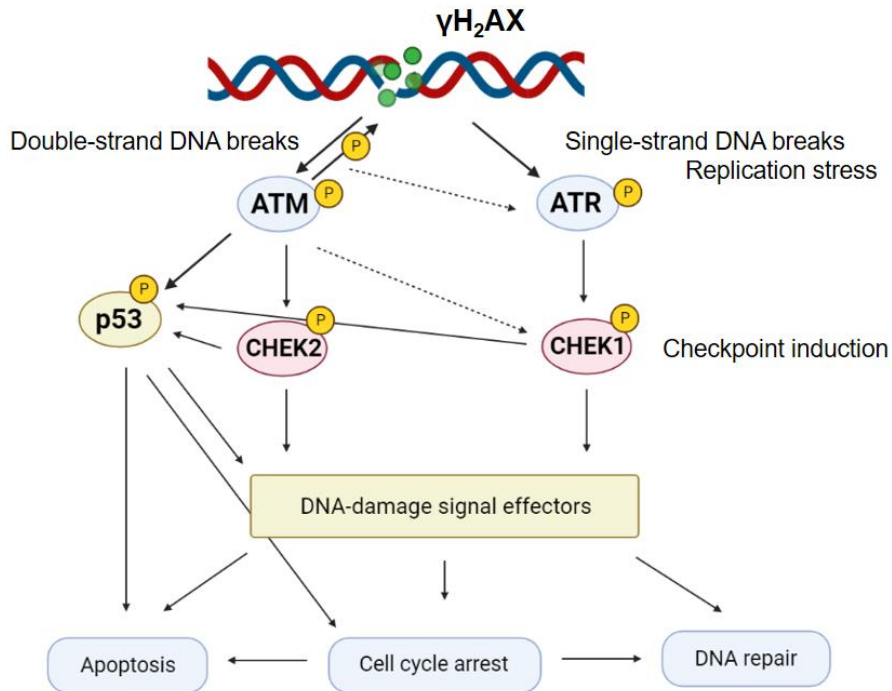


Figure 7. γ H2AX, key molecular marker of DNA damage response. DNA damage is recognized by γ H2AX as it initiates the DNA repair system. H2AX is phosphorylated by the protein kinase ATM which is activated in response to DSB. H2AX can also be phosphorylated by ATR. ATR phosphorylates H2AX in response to single-stranded DNA breaks and during replication stress. The ATM and ATR are central to the DNA damage response. Downstream of these proteins are two families of checkpoint kinases (CHEK), the CHEK1 and CHEK2 kinases. Below this level of signal transduction are the effectors that execute the functions of the DNA damage response.¹⁸

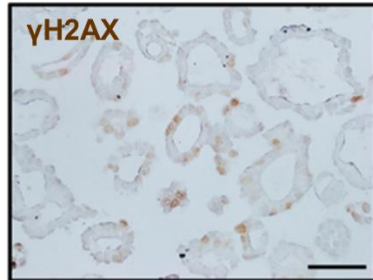
8. DNA Damage Responses (DDR) of PDOs to MNNG and O⁶BG

To evaluate the expression of γ H2AX in normal, MLH1 mutated and MSH2 mutated patient-derived organoids, we treated MNNG (25 μ M) or combination of MNNG (25 μ M) and O⁶BG (25 μ M). Then, we confirmed the expression of γ H2AX by immunohistochemistry (figure 8A), western blot (figure 8B) and immunofluorescence (figure 8C). We performed immunofluorescence in normal organoids from 6 patients, MLH1 mutated organoids from 5 LS-patients and MSH2 mutated organoids from 5 LS-patients (figure 8 D-F). Thus, we found the increased γ H2AX expression after treatment of MNNG or combination of MNNG and O⁶BG in normal organoids. However, the PDOs with the MMR gene mutation showed no or less DNA damage responses after the drug treatment, compared to normal organoids.

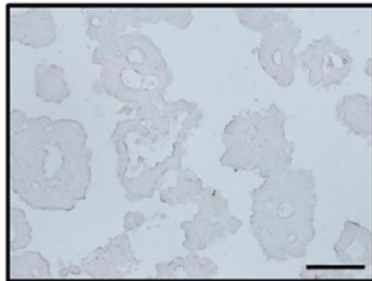
A.

2 μ M MNNG

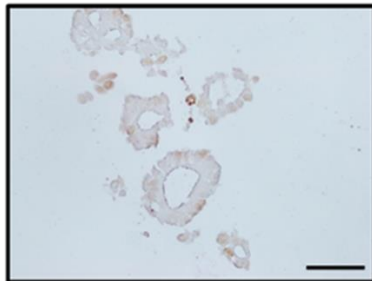
Normal
organoid



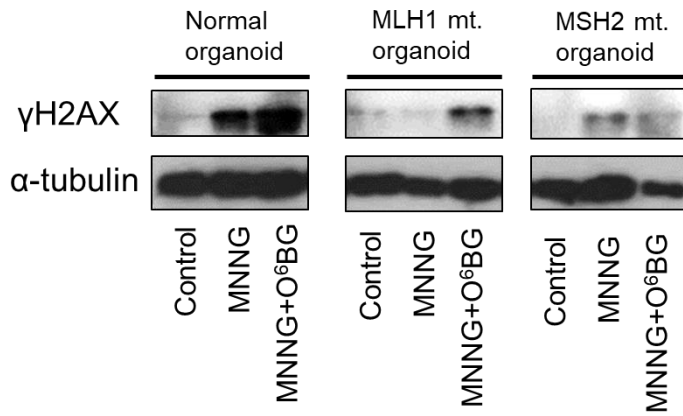
MLH1 mutation
Organoid



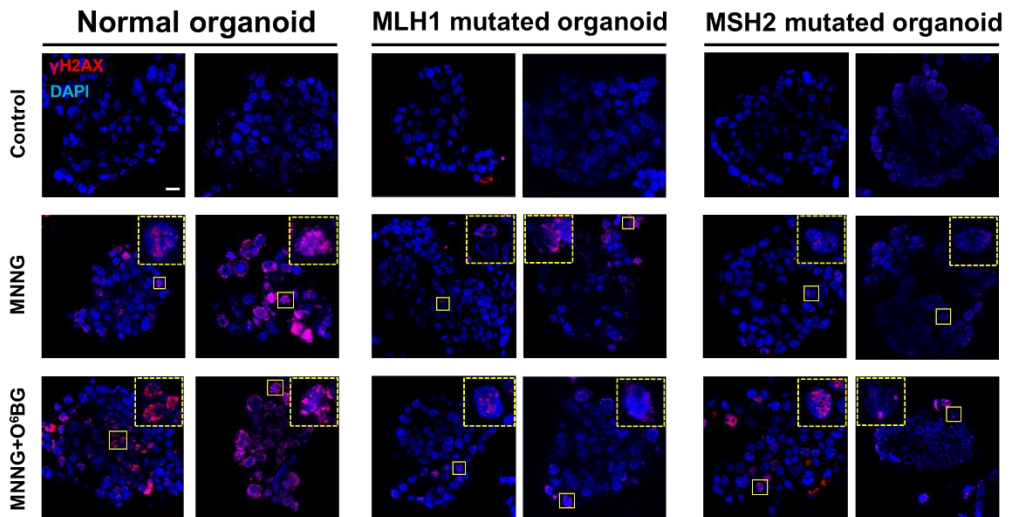
MSH2 mutation
Organoid



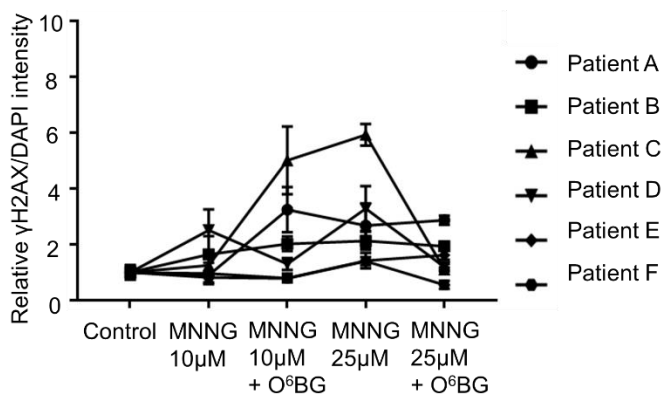
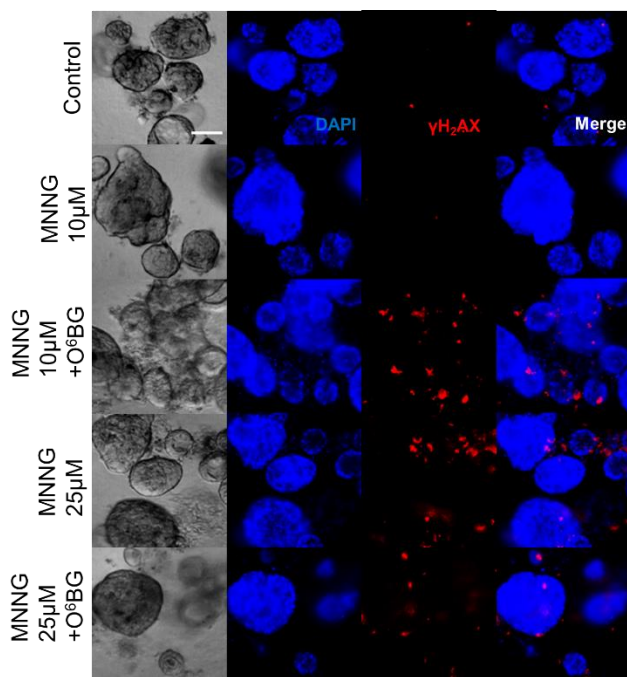
B.



C.



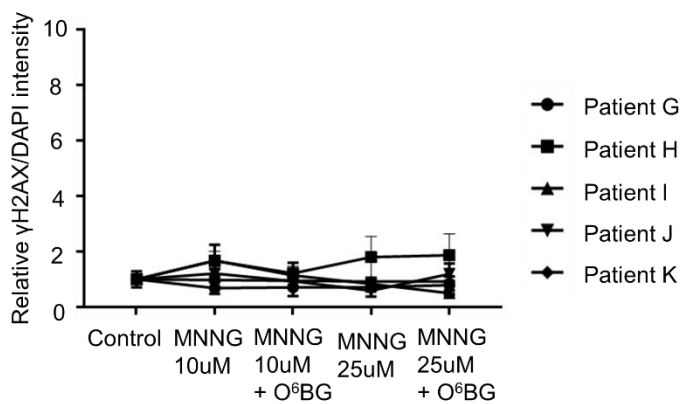
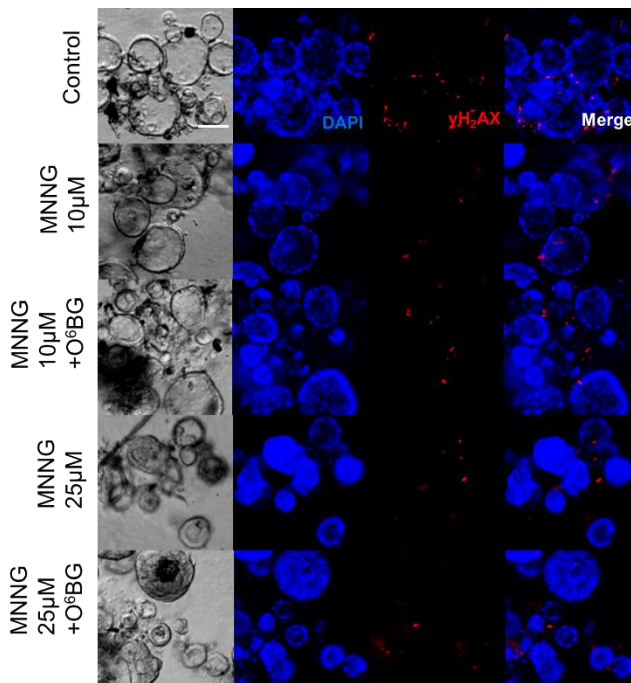
D.



	MNNG 10μM	MNNG 10μM + O ⁶ BG	MNNG 25μM	MNNG 25μM + O ⁶ BG
Patient A	n.s (0.5647)	* (0.0077)	* (0.018)	*** (0.0009)
Patient B	n.s (0.2235)	* (0.0160)	* (0.0218)	*** (0.0003)
Patient C	n.s (0.1784)	n.s (0.1332)	** (0.0016)	n.s (0.1017)
Patient D	n.s (0.0607)	n.s (0.1199)	* (0.0309)	n.s (0.2175)
Patient E	n.s (0.8714)	n.s (0.2136)	n.s (0.0595)	* (0.0064)
Patient F	n.s (0.2514)	n.s (0.0608)	* (0.0225)	* (0.0138)

*p<0.05, **p<0.01, ***p<0.001, compared with the control

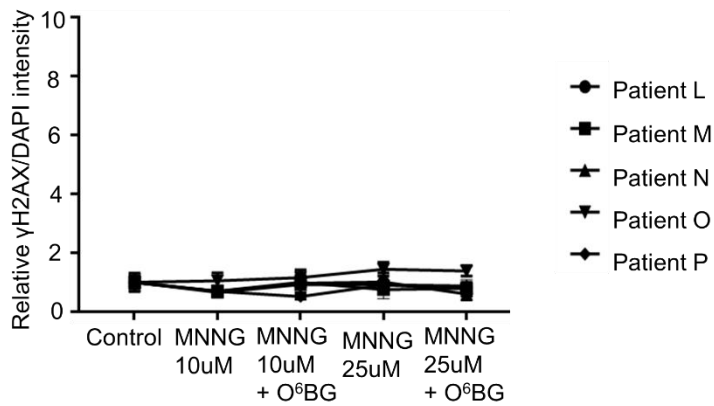
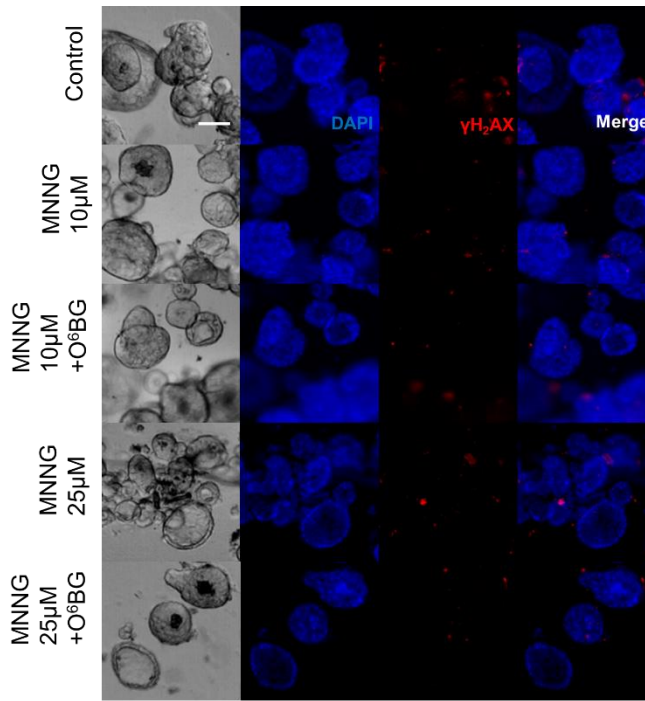
E.



	MNNG 10µM	MNNG 10µM + O ⁶ BG	MNNG 25µM	MNNG 25µM + O ⁶ BG
Patient G	n.s (0.1003)	n.s (0.1802)	n.s (0.2053)	n.s (0.3056)
Patient H	* (0.0260)	n.s (0.1604)	n.s (0.1176)	n.s (0.1084)
Patient I	n.s (0.1662)	n.s (0.6167)	n.s (0.4530)	n.s (0.0894)
Patient J	n.s (0.3331)	n.s (0.6012)	* (0.0157)	n.s (0.3827)
Patient K	n.s (0.4711)	n.s (0.0598)	n.s (0.1426)	** (0.0017)

*p<0.05, **p<0.01, **p<0.001, compared with the control

F.



	MNNG 10µM	MNNG 10µM + O ⁶ BG	MNNG 25µM	MNNG 25µM + O ⁶ BG
Patient L	* (0.0316)	n.s (0.8441)	n.s (0.9522)	* (0.0436)
Patient M	n.s (0.1516)	n.s (0.9853)	n.s (0.3320)	n.s (0.4917)
Patient N	n.s (0.1202)	n.s (0.7620)	n.s (0.6542)	n.s (0.5011)
Patient O	n.s (0.7492)	n.s (0.3699)	* (0.0304)	* (0.0327)
Patient P	* (0.0261)	* (0.0049)	n.s (0.3926)	n.s (0.0711)

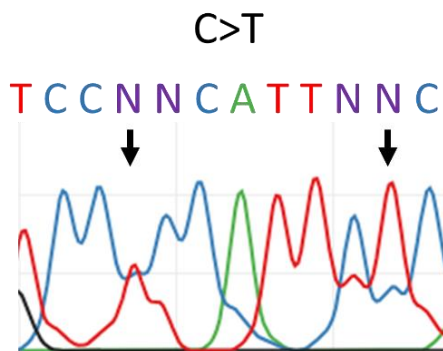
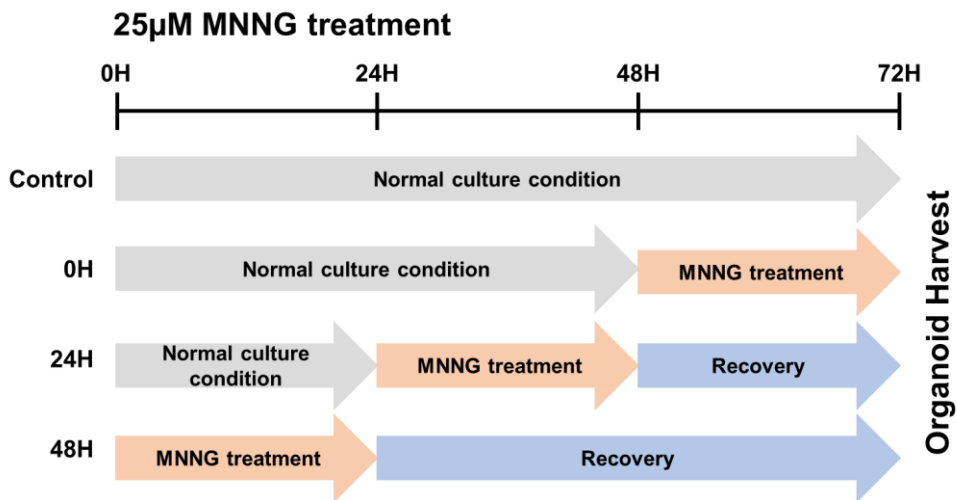
*p<0.05, **p<0.01, ***p<0.001, compared with the control

Figure 8. γ H2AX expression after treatment of MNNG and O⁶BG in normal and LS-PDOs. (A) Immunohistochemical staining, (B) western blot analysis and (C) immunofluorescence staining for γ H2AX expression were performed in normal organoids and MLH1/MSH2 mutated LS-PDOs after treatment of 2 μ M MNNG or 25 μ M MNNG and O⁶BG for 24 hours. Scale bar, 50 μ m (A) and 20 μ m (C). (D-F) The expression of γ H2AX after MNNG and O⁶BG treatment were measured by immunofluorescence in normal organoid (D), MLH1 mutated organoid (E) and MSH2 mutated organoid (F) LS-PDOs. (top, the immunofluorescence images of organoids after drug treatment; bottom, relative γ H2AX/DAPI intensity curves after drug treatment) Scale bar, 100 μ m. Data were expressed as the mean \pm standard error of three independent experiments; * $p < 0.05$, ** $p < 0.01$, and *** $p < 0.001$ (compared with the control).

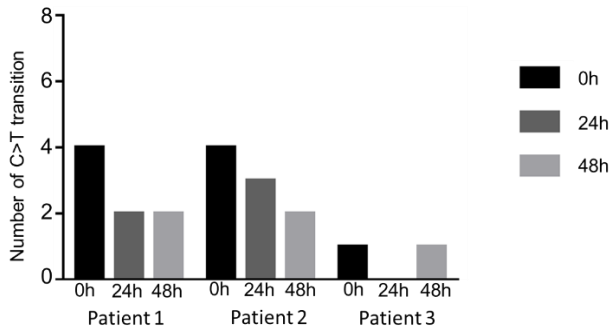
9. MNNG-induced mutation accumulation in normal organoids and LS-PDOs

MNNG induces O⁶-meG and it pairs with thymine mismatch, and the MNNG-treated cells initially show C>T base transitions. Therefore, we performed Sanger sequence analysis to identify the mutations accumulated by MNNG. To clearly identify the base transitions, we targeted sequences in 2 sites of CpG island of APC gene. The organoids were treated with 25 μ M MNNG for 24 hours and harvested after 0 hour, 24 hours and 48 hours. As expected, after the MNNG treatment, MLH1 and MSH2 mutated LS-PDOs showed an increased C>T base transitions over time, compared to normal organoids.

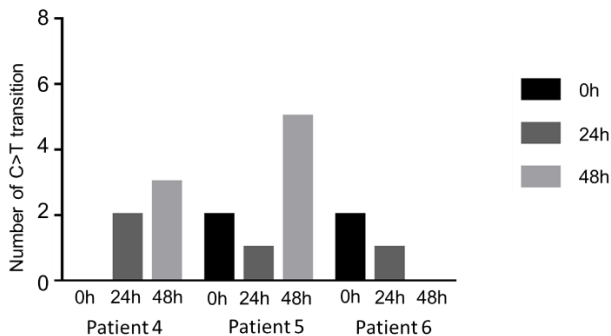
A.



B.



C.



D.

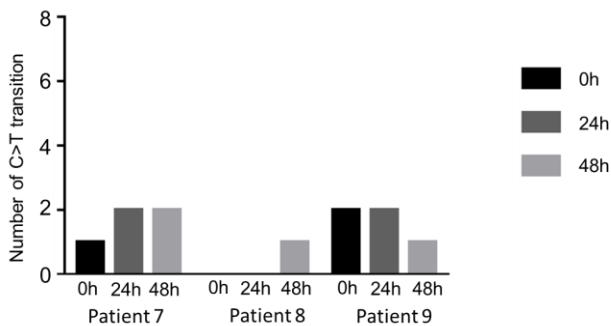


Figure 9. MNNG-induced Single Nucleotide Variants(SNVs) in normal organoids and LS-PDOs. (A) A schematic diagram of drug treatment and organoid harvest with recovery time (top), Sanger sequencing analysis of C>T transitions (bottom). The accumulated number of C>T transition of normal (B), MLH1 mutated (C) and MSH2 mutated (D) organoids with 25 μ M MNNG treatment.

Table1. Primer sequences for CpG island in APC gene.

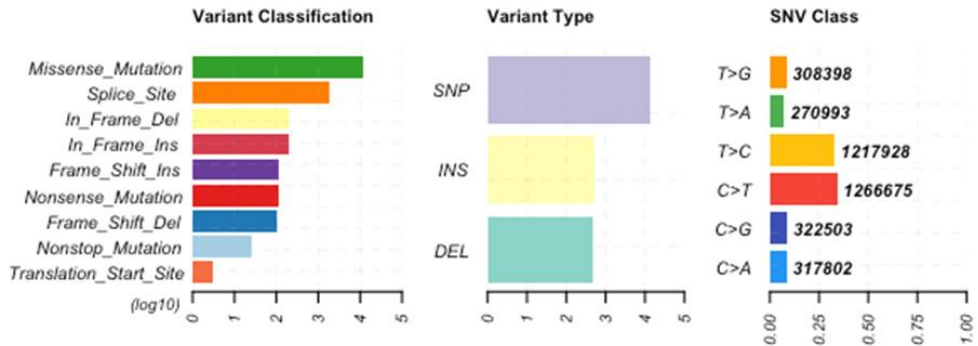
Target	Primer Sequence(5' to 3')	GC%	Length
APC_CpG_1	Forward: AGACAAACAAGGATTTCCCGGAAGA	57	1430
	Reverse: AGATGAACAATCATTTGCCAACAGA		
APC_CpG_2	Forward: TCATCACTCTGACAACACTCAGTGACT	54	923
	Reverse: GCTCCTCGCCATGAATATGCTC		

10. Whole genome sequence analysis in MNNG-treated normal organoids and MLH1 mutated PDOs

To identify the mutations that accumulated by MNNG, the normal organoid and MLH1 mutated LS-PDO were subjected to whole genome sequencing(WGS) analysis after treatment of MNNG. We treated 25 μ M of MNNG in normal and MLH1 mutated PDOs for 24 hours and cultured without MNNG for 48 hours to allow organoids to accumulate or recover mutations. The mutation is accumulated in MLH1-deficient organoids, which is driven by replication errors.¹⁹ Both MNNG-treated and untreated organoids were subjected to WGS analyses to identify the mutations that accumulated in the normal and MLH1 mutated PDOs. The MNNG-treated normal organoids showed a decreased number of base substitution compared to MNNG-untreated organoids. However, the MLH1 mutated organoids showed an increased number of base substitution in MNNG treatment, compared to MNNG-untreated organoids. This confirmed that pathogenic mutation of MLH1 gene induced the generation of mutations by dysfunction of mismatch repair.

A.

Control

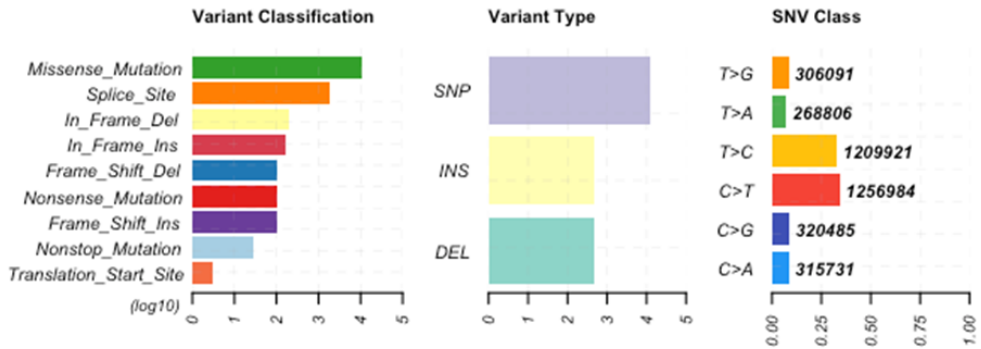


MNNG treatment



B.

Control



MNNG treatment

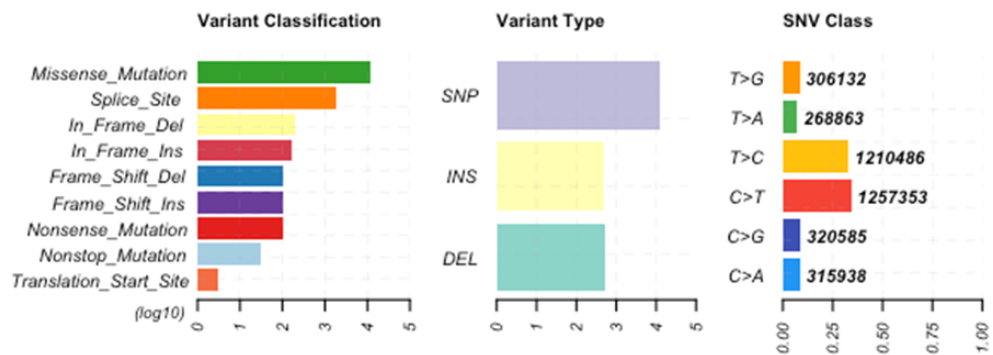


Figure 10. MNNG-induced Mutation analysis in normal and MLH1 mutated PDOs. Number of mutations accumulated in normal organoids (A) and MLH1 mutated organoids (B) in both MNNG-treated and untreated condition was measured by WGS. Shown are variants subdivided by mutation type, SNP, INDELS and base substitutions. (top, the analysis of mutations MNNG-untreatment; bottom, the analysis of mutations after 25 μ M MNNG treatment for 24 hours and recovery for 48 hours)

IV. DISCUSSION

Although LS patients have a high risk of CRC, they have various risk of developing CRC.²⁰ The LS is caused by inherited mutations in genes of the DNA mismatch repair (MMR) pathway, which has been remarkably important for the management of this disease. However, the proper risk assessment that evaluates the cancer risk of LS patients has not been established. Also, a proper diagnosis, prevention approaches, and appropriate decisions for LS including aggressive CRC patients are needed. Therefore, detailed molecular information about the MMR pathway has been essential for guiding the diagnosis of LS. Recently, it has been reported that the MMR-deficient cells are more resistant to the cytotoxic effects of certain DNA damage agents. In particular, Karran P. et al demonstrated that MMR-deficient *E.coli* were shown to be resistant to the cytotoxic effects of the DNA alkylating agent N-methyl-N'-nitro-N-nitrosoguanidine (MNNG).²¹ MNNG has been used to induce DNA methylation damage that is directly recognized by MMR proteins, which results in recruitment of MMR genes. Thus, the critical cytotoxic lesion created by MNNG is the O⁶-methylguanine, which is commonly mispaired with thymine during replication resulting in a MeG-T mispair. Then MMR-related genes recognize and remove these lesions, and methylguanine methyltransferase (MGMT) also directly repairs methylguanine. Thus, the processing of a MeG-T mispairs by the MMR pathway creates secondary DNA damage that ultimately causes cell death. In addition to the futile cycle model, researchers have demonstrated protein-protein interactions between the MMR proteins and key DNA damage signaling molecules such as ATR, ATM, CHK1, and CHK2. These mechanisms indicate that MMR plays a protective role in repairing and removing damaged cells to reduce the risk of mutation accumulation.

Using these detailed molecular mechanisms of MMR pathway, we came to identify some factors to be considered for developing an individualized model to predict CRC risk in LS.

As for the biological significance of MMR genes, some researchers showed functional assays in different experimental systems. However, most of them have

intrinsic limitations because they were developed based on bacteria, yeast, or mice.⁷

Recently, Bouvet D et al. reported that an assay for measuring cell response to the cytotoxic effect of a methylating agent can determine the effects of VUS in MMR genes. Based on the DNA damage-induced apoptosis function of MMR, they evaluated the significance of VOUS of MMR genes, using a large panel of 88 variants, mainly missense variants, including a validation set of 40 previously classified variants and a prospective set of 48 VUS.⁶ However, this assay also measured only restrictive cell biological properties of variant MMR protein levels.

Therefore, we used LS-PDOs to reflect their own other molecules to be related to the MMR pathway and its consequence. Then, to maximize the difference in MNNG-induced cytotoxicity of organoids, we used an ATR inhibitor. In addition, to investigate the functional activity of MGMT to repair methylguanine and suppress their function to show more MMR-dependent pathways, O⁶BG, an MGMT inhibitor, was used in our models. Therefore, we utilized normal organoids and LS-PDOs treated with ATR inhibitor and O⁶BG to maximize the difference in MNNG-induced cytotoxicity. Then, in the PDO model for earlier detection of DDR using γ H2AX, organoids were treated with MNNG alone and MNNG/O⁶BG, and without ATR inhibition to detect DDR in live cells.

From our results, we demonstrated that MMR gene mutated LS-PDOs could survive in MNNG-induced DNA lesions and segmented cell death, which suggest the association with high cancer risk.

However, to confirm the difference of MNNG-induced cytotoxicity in PDOs, long-term culture of organoids for several passages was needed. Therefore, to detect DNA damage in an earlier phase, we utilized a DNA damage recognition marker, γ H2AX. Normal organoids showed high DDR by MNNG and O⁶BG treatment. However, the MMR gene mutated organoids showed a much less DDR. Our results enabled the discrimination of early phase DDR damaged by MNNG and O⁶BG between normal and LS patients. Then, we confirmed the difference in mutation accumulation

between normal and LS-PDOs by Sanger sequencing analysis of CpG island site, and WGS in the same condition of drug treatment. In addition, our analysis of sequencing data allowed us to define a mutational signature of MMR deficiency.

However, even in normal organoids, there were various MNNG-induced DDR changes. Therefore, we need to explain these variations by IHCS of MMR proteins to confirm the correlation between DDR and MMR protein expression levels in normal organoids.²²

In addition, recently, Lena Bohaumilitzky, et al., (2022) demonstrated an increased T-cell infiltrate in the normal colon mucosa of MSI CRC patients and healthy LS carriers compared with MSS CRC patients.²³ LS carriers showed elevated mucosal T-cell infiltration even without cancer. These results suggest that we have to consider the factor of immune rejection as a protective factor against CRC risks in LS patients in future studies.

Further research using larger sample sizes with long-term prognostic clinical data and various genetic mutations associated with LS is needed to confirm that our PDO model is suitable for CRC risk prediction in LS patients. In addition, Jarno Drost, et al have shown that the pre-dominant mutation profiles observed in MLH1 deleted organoids by using CRISPR/Cas9 technology.¹⁹ This technology also could be useful to investigate the biological and clinical significance of MMR genes.

Moreover, our PDO model can be applied to biological validation of VOUS, and individualized cancer risk prediction models of other tumors, such as endometrial and gastric cancer as well.

V. CONCLUSION

In conclusion, we demonstrated that MNNG-induced DNA damage and cell death were different between normal organoid and LS-PDOs, suggesting that our PDO model could serve as a useful individualized prediction model for CRC risk in LS patients.

REFERENCES

1. Siegel RL, Miller KD, Goding Sauer A, Fedewa SA, Butterly LF, Anderson JC, et al. Colorectal cancer statistics, 2020. *CA: a cancer journal for clinicians* 2020;70:145-64.
2. Nguyen HT, Duong HQ. The molecular characteristics of colorectal cancer: Implications for diagnosis and therapy. *Oncology letters* 2018;16:9-18.
3. Boland CR, Goel A. Microsatellite instability in colorectal cancer. *Gastroenterology* 2010;138:2073-87. e3.
4. Bhattacharya P, McHugh TW. Lynch syndrome. *StatPearls* [Internet]: StatPearls Publishing; 2021.
5. Dowty JG, Win AK, Buchanan DD, Lindor NM, Macrae FA, Clendenning M, et al. Cancer risks for MLH 1 and MSH 2 mutation carriers. *Human mutation* 2013;34:490-7.
6. Bouvet D, Bodo S, Munier A, Guillerm E, Bertrand R, Colas C, et al. Methylation tolerance-based functional assay to assess variants of unknown significance in the MLH1 and MSH2 genes and identify patients with Lynch syndrome. *Gastroenterology* 2019;157:421-31.
7. Carethers JM, Hawn MT, Chauhan DP, Luce MC, Marra G, Koi M, et al. Competency in mismatch repair prohibits clonal expansion of cancer cells treated with N-methyl-N'-nitro-N-nitrosoguanidine. *The Journal of clinical investigation* 1996;98:199-206.
8. Boland CR. Roles of the DNA mismatch repair genes in colorectal tumorigenesis. *International journal of cancer* 1996;69:47-9.
9. Stojic L, Brun R, Jiricny J. Mismatch repair and DNA damage signalling. *DNA repair* 2004;3:1091-101.
10. Scherer S, Avdievich E, Edelmann W. Functional consequences of DNA mismatch repair missense mutations in murine models and their impact on cancer predisposition. *Biochemical Society Transactions* 2005;33:689-93.
11. Guillotin D, Martin SA. Exploiting DNA mismatch repair deficiency as a therapeutic strategy. *Experimental cell research* 2014;329:110-5.
12. Meyers M, Hwang A, Wagner MW, Boothman DA. Role of DNA mismatch repair in apoptotic responses to therapeutic agents. *Environmental and molecular mutagenesis* 2004;44:249-64.
13. Fu D, Calvo JA, Samson LD. Balancing repair and tolerance of DNA damage caused by alkylating agents. *Nature Reviews Cancer* 2012;12:104-20.
14. Wyatt MD, Pittman DL. Methylating agents and DNA repair responses: Methylated bases and sources of strand breaks. *Chemical research in toxicology* 2006;19:1580-94.
15. Casorelli I, Russo MT, Bignami M. Role of mismatch repair and MGMT in response to anticancer therapies. *Anti-Cancer Agents in*

- Medicinal Chemistry (Formerly Current Medicinal Chemistry–Anti-Cancer Agents) 2008;8:368–80.
16. Gupta D, Lin B, Cowan A, Heinen CD. ATR–Chk1 activation mitigates replication stress caused by mismatch repair–dependent processing of DNA damage. *Proceedings of the National Academy of Sciences* 2018;115:1523–8.
 17. Celeste A, Fernandez–Capetillo O, Kruhlak MJ, Pilch DR, Staudt DW, Lee A, et al. Histone H2AX phosphorylation is dispensable for the initial recognition of DNA breaks. *Nature cell biology* 2003;5:675–9.
 18. Maréchal A, Zou L. DNA damage sensing by the ATM and ATR kinases. *Cold Spring Harbor perspectives in biology* 2013;5:a012716.
 19. Drost J, Van Boxtel R, Blokzijl F, Mizutani T, Sasaki N, Sasselli V, et al. Use of CRISPR–modified human stem cell organoids to study the origin of mutational signatures in cancer. *Science* 2017;358:234–8.
 20. Volkova NV, Meier B, González–Huici V, Bertolini S, Gonzalez S, Vöhringer H, et al. Mutational signatures are jointly shaped by DNA damage and repair. *Nature communications* 2020;11:1–15.
 21. Karran P. Mechanisms of tolerance to DNA damaging therapeutic drugs. *Carcinogenesis* 2001;22:1931–7.
 22. McCarthy AJ, Capo–Chichi JM, Spence T, Grenier S, Stockley T, Kamel–Reid S, et al. Heterogenous loss of mismatch repair (MMR) protein expression: a challenge for immunohistochemical interpretation and microsatellite instability (MSI) evaluation. *The Journal of Pathology: Clinical Research* 2019;5:115–29.
 23. Bohaumilitzky L, Kluck K, Hüneburg R, Gallon R, Nattermann J, Kirchner M, et al. The different immune profiles of normal colonic mucosa in cancer–free Lynch syndrome carriers and Lynch syndrome colorectal cancer patients. *Gastroenterology* 2022;162:907–19. e10.

ABSTRACT(IN KOREAN)

불일치 복구 유전자의 생식세포 돌연변이 환자에서 환자 유래
오가노이드 모델을 이용한 대장암 위험도 예측

<지도교수 김태일>

연세대학교 대학원 의과학과

신유미

대장암(CRC)의 약 10~15%가 현미부수체 불안정성(MSI) 증양을 보이고, MSI 증양의 약 20%가 '린치증후군 (Lynch syndrome)' 또는 '유전성 비용종증 결장직장암 증후군 (HNPCC)'으로 알려진 불일치 복구 (MMR) 유전자 MLH1, MSH2, MSH6, PMS2, EPCAM의 생식선 돌연변이에 의해 발생된다.

린치증후군 환자는 대장암 발병 위험이 높지만, 린치증후군 환자에서 암위험도는 실제 다양하게 나타나며, 암위험도를 예측할 수 있는 효과적인 모델이 없다. 따라서, 우리는 린치 증후군 환자 유래 오가노이드 (PDO)를 이용한 대장암 발병 위험도에 대한 개별화된 예측 모델을 개발하고자 한다.

우선 DNA 손상 유발 세포사멸반응을 기반으로 메틸화제인 N-메틸-N'-니트로-N-니트로소구아니딘 (MNNG)의 세포독성 효과에 대한 오가노이드 반응을 측정했다. 정상 대장 오가노이드에서 고농도/단기간 및 저농도/장기간의 MNNG를 처리하였고, 오가노이드 크기는 상대적으로 감소했지만 갯수에는 큰 차이를 보이지 않았다. MNNG의 효과를 높이고 대장 오가노이드의 세포 사멸을 유도하기 위해 O⁶BG와 ATR 억제제를 추가로 처리하였다. MNNG, O⁶BG 및 ATR 억제제를 같이 처리함으로써 세포독성 효과에서 MMR 유전자 돌연변이 오가노이드에 비해 정상 오가노이드가 민감하다는 것을 발견했다. 더 이른 단계에서의 빠른 변화의 차이 확인을 위해 DNA 손상 인식 마커인 γ H2AX의 발현을 분석하여 DNA 손상 반응을 조사하였다. MGMT 억제제인 MNNG와

O⁶BG를 처리한 후, MMR 유전자 돌연변이 오가노이드보다 정상 오가노이드에서 γ H2AX의 높은 발현을 발견했다. 또한, MNNG에 의해 유도된 돌연변이 수가 정상 오가노이드에 비해 MMR 유전자 돌연변이 오가노이드에서 상당히 증가하는 것을 발견했다.

MNNG에 의해 축적된 돌연변이를 확인하기 위해, 생어시퀀싱 분석과 전장유전체분석 (Whole Genome Sequencing)을 진행하였다. 대장 오가노이드에 MNNG를 처리하고, 여러 회복 시간 별로 오가노이드를 얻어 분석을 진행하였다. 정상 오가노이드에서 시간에 따라 감소되는 염기 전위들을 발견할 수 있었지만 반면에, MMR 유전자 돌연변이 오가노이드에서는 증가되는 것을 발견했다. 더불어, 전장유전체분석 결과를 통해, MNNG에 의해 유도된 돌연변이 숫자가 MLH1 유전자 돌연변이 오가노이드에서 정상 오가노이드에 비해 상당히 증가되는 것을 발견하였다.

결론적으로, 린치 증후군 환자 유래 오가노이드 모델에서 MNNG와 O⁶BG에 의한 DNA 손상 반응 측정은 대장암 위험의 개별화된 예측 모델이 될 수 있다.

핵심되는 말 : 환자 유래 오가노이드, 대장암, 린치신드롬, DNA 손상 반응, MNNG